PCCP

PAPER

View Article Online
View Journal | View Issue

Cite this: *Phys. Chem. Chem. Phys.*, 2022, **24**, 2958

Brownian dynamics of cylindrical capsule-like particles in a nanopore in an electrically biased solid-state membrane

Craig C. Wells, Dmitriy V. Melnikov and Maria E. Gracheva *

We use Brownian dynamics simulations to study the motion of cylindrical capsule-like particles (capsules) as they translocate through nanopores of various radii in an electrically biased silicon membrane. We find that for all pore sizes the electrostatic interaction between the particle and the pore results in the particle localization towards the pore 's center when the membrane and the particle have charges of the same sign (case 1) while in case of the opposite sign charges, the capsule prefers to stay near and along the nanopore wall (case 2). The preferential localization leads to all capsules rotating less while inside the pore compared to the bulk solution, with a larger net charge and/or particle length resulting in a smaller range of rotational movement. It also strongly affects the whole translocation process: in the first case, the translocation is due to the free diffusion along the pore axis and is weakly dependent on the particle charge and the nanopore radius while in the second case, the translocation time dramatically increases with the particle size and charge as the capsule gets "stuck" to the nanopore surface.

Received 29th August 2021,
Accepted 14th January 2022

DOI: 10.1039/d1cp03965b

rsc.li/pccp

1 Introduction

The detection and characterization of biomolecules[1–5] has been a growing field of interest with an increase in number of research studies focused on nanopore-based applications and the advancement of biosensing technologies.[6–11] This rapid nanopore-based identification technology is frequently made possible by analyzing the ionic current blockade trace produced by a molecule translocating a nanopore embedded in a membrane.[12–19] A system such as this works by having the nanoporous membrane separate two chambers filled with electrolyte solution, one where biomolecules initial reside in (the *cis* chamber), and the chamber they are encouraged to translocate into (the *trans* chamber) *via* the nanopore.

Nanopores can also be utilized with particles whose shape and orientation affect the ionic current trace in a way that may be more difficult to interpret, such as for a non-globular molecule like a cylinder or capsule. In particular, cylinder-shaped particles have been the focus of several investigations.[15,16,20–26] For example, one experimental study[15] focused on unique features of the ionic current profile for a rod-shaped, silicon dioxide particle translocating a nanopore with irregularities to distinguish objects of different shapes. The results of the same investigation suggest that the rods will rotate while translocating the nanopore. Another study[16] found that nanorods will tumble (a "tumble" refers to the capsule's major axis rotating over itself in the direction of the pore axis) while translocating a glass nanopipet, thus resulting in a current blockade dependent on the rod's angular orientation. In general, however, analysis of ionic current traces for these particles proved to be a challenge due to their unique shape and motion[27].

One way to further our understanding of particle transloctaion dynamics is by employing computational modelling. This way, it is possible to investigate fine features of the molecule translocation process that would otherwise be difficult to observe experimentally. There are many ways to approach a nanopore system *via* modelling, from extremely detailed atomic level models[28,29] to simpler models that yield broader statistical information on the system.[30–33] Atomic level modelling can be expensive in computational resources and time, while modelling particles using Brownian dynamics (BD) and rigid, coarse-grained structures[34] considerably reduces the computational cost and provides a good agreement with atomic level approaches.

In this work, the translocation dynamics of cylindrical capsule-like particles (hereby referred to as capsules) is studied using a BD model. Particles of various lengths and charges are studied to explore how each affects the particle's behavior in the pore. Additionally, different pore sizes and electric biases applied to the membrane are investigated to understand how the electric environment modifies the particle's movement.[35,36]

Department of Physics, Clarkson University, Potsdam, NY 13699, USA.
E-mail: gracheva@clarkson.edu

This work is organized as follows: The particle, system, and the computational model are described in Section 2. In Section 3, the results of our simulations are presented and discussed. Our findings are then summarized in Section 4.

2 Method

We consider a semiconductor membrane made of silicon (Si) with an 8 Å thick negatively charged surface layer of silicon dioxide (SiO_2) with volume charge density of -4×10^{20} e cm^{-3} (corresponding to a surface charge density of -0.32 e nm^{-2}), where e is the elementary charge. An aqueous KCl electrolyte solution of bulk concentration C_{KCl} = 0.1 M fills a *cis* and *trans* chambers separated by the L = 260 Å thick membrane and connected by a cylindrical nanopore of radius R_p = 40 Å to 60 Å as shown in Fig. 1. A capsule is initially placed in the *cis* chamber, requiring it to translocate the nanopore to move into the *trans* chamber. An electric bias of $V_m = \pm 1$ V is applied to Si, resulting in a positive or negative overall effective surface charge, respectively.[37,38] The system's electric potential, $\phi(\mathbf{r})$, is numerically calculated using the Poisson–Nernst–Planck (PNP) approach, as described in our previous works.[35,39] The dependence of the electric potential and electric field in and around the nanopore on the applied membrane bias and membrane surface charge are discussed in greater detail elsewhere.[37,38]

In this work, we approximate a capsule of various length and charge through a coarse-grained method developed earlier[36,38] and illustrated in Fig. 2. A capsule particle is comprised of N overlapping spheres (N ranges from 3 to 11) fixed in relative positions as a rigid body where each sphere has a radius R_b = 5 Å

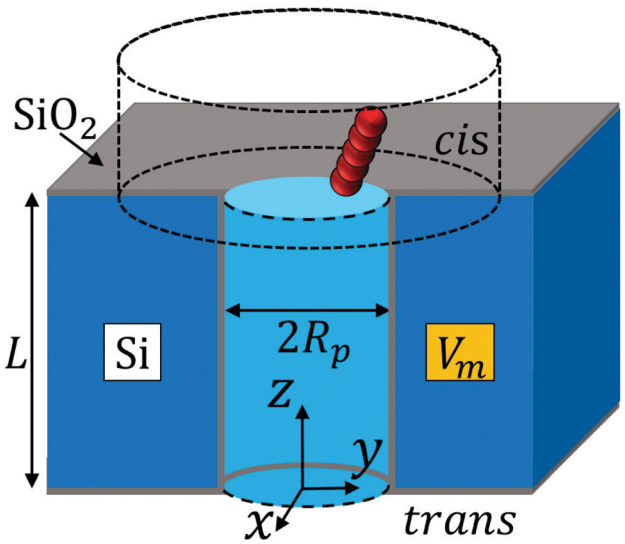

Fig. 1 Schematic diagram of the simulated system (not to scale). The silicon membrane with electric bias of V_m is covered by a negatively charged layer of silicon dioxide. The particle's movement is restricted by a large bounding box while in the *cis* chamber, represented by the dashed lines above the pore. The membrane reference frame with x, y, and z-axes originates at the bottom, center of the pore.

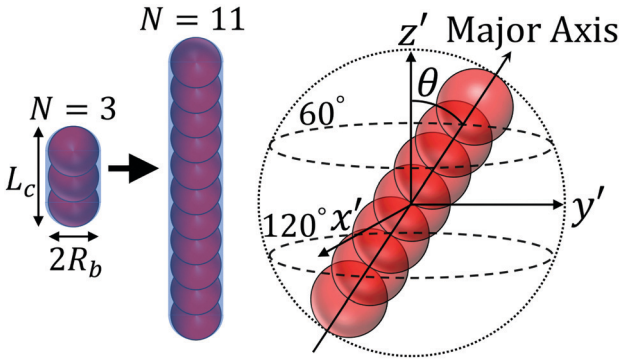

Fig. 2 The simulated capsule and its center of mass reference frame (x', y', z'). Capsule orientation angle θ is the angle between the +z'-direction and the capsule's major axis.

and a point charge $q_i = 0, -1e, -2e$ concentrated at each sphere's center. The ratio between the particle's length L_c and width $2R_b$, $p = \frac{L_c}{2R_b} = \frac{N+1}{2}$, can be used to define the perpendicular/parallel translational and the rotational drag coefficients relative to the capsule's major axis as:[40,41]

$$\xi_\perp = \frac{4\pi\eta L_c}{\ln(p) + 0.839 + 0.185/p + 0.233/p^2}, \quad (1)$$

$$\xi_\parallel = \frac{2\pi\eta L_c}{\ln(p) - 0.207 + 0.980/p - 0.133/p^2}, \quad (2)$$

$$\xi_R = \frac{\pi\eta L_c^3/3}{\ln(p) - 0.662 + 0.917/p - 0.050/p^2}, \quad (3)$$

where $\eta = 10^{-3}$ Pa s is the solution viscosity.

The movement of the capsule in the nanoporous system is simulated using BD approach, discussed fully in our previous studies[36,42] and is similar to the method developed in ref. 41. The translational motion of the particle's center of mass position $\mathbf{r}_{cm}(t)$[36] in the directions parallel and perpendicular to the capsule's major axis can be determined as

$$r_{cm\parallel}(t) = r_{cm\parallel}(t - \delta t) + \sum_{i=1}^{N} F_{i\parallel}\frac{\delta t}{\xi_\parallel} + \sqrt{\frac{6\delta t k_b T}{\xi_\parallel}}\mathbf{n}_\parallel, \quad (4a)$$

$$\mathbf{r}_{cm\perp}(t) = \mathbf{r}_{cm\perp}(t - \delta t) + \sum_{i=1}^{N} \mathbf{F}_{i\perp}\frac{\delta t}{\xi_\perp} + \sqrt{\frac{6\delta t k_b T}{\xi_\perp}}\mathbf{n}_\perp, \quad (4b)$$

where $\mathbf{r}_{cm}$ = ($r_{cm\parallel}$, $\mathbf{r}_{cmp}$), $\mathbf{n}_T$ = ($n_\parallel$, $\mathbf{n}_p$) is a random three-dimensional vector with components uniformly distributed between interval [−1, 1],[38,43,44] δt = 1.0 ps is the time step, and the position of each bead $\mathbf{r}_i$, i = 1,..., N is then updated in the membrane reference frame. In eqn (4a) and (4b), the second term is due to the net external forces $\mathbf{F}_i$ = ($F_{i\parallel}$, $\mathbf{F}_{i\perp}$) computed at the previous time step $t - \delta t$ and applied to each bead. This force is due to the hard-sphere particle-membrane Lennard-Jones (LJ) interaction energy with LJ radii of 2.5 Å and the electrostatic potential energy, $q_i\phi(\mathbf{r}_i)$.[35,42] The last term of eqn (4a) and (4b) describes stochastic effects on translational

motion. Since the external electrolyte bias is held at zero, the hydrodynamic force on the particle is negligible and omitted.

Due to the capsule shape of the particle, rotational Brownian motion must be considered to accurately model its change in orientation. This change is effectively described by the angle $\delta\boldsymbol{\Omega}$ by which particle's major axis turns and which in the center of mass (x', y', z') coordinate system can be computed as[36]:

$$\delta\boldsymbol{\Omega} = \sum_{i=1}^{N} (\mathbf{r}_i - \mathbf{r}_{cm}) \times \mathbf{F}_i \frac{\delta t}{\xi_R} + \sqrt{\frac{6\delta t k_b T}{\xi_R}} \mathbf{n}_R. \quad (5)$$

Here, the first term represents the net torque due to external forces, determined by the same potential energies as in eqn (4a) and (4b) and the second term is a random torque responsible for stochastic rotation.

3 Results and discussion

3.1 Capsule's position and orientation inside the nanopore

Using the above BD approach, we study how membrane potentials of $V_m = \pm 1$ and nanopores with radii of R_p = 40 Å, 44 Å, 48 Å, 52 Å, 56 Å, and 60 Å affect the dynamics of capsules constructed of N = 3, 5, 7, 9, and 11 beads where all beads have the same radius of R_b = 5 Å (capsule length L_c = 20 Å, 30 Å, 40 Å, 50 Å, and 60 Å) and the same bead charge of q_i = 0, $-1e$ or $-2e$. A single simulation starts with the particle placed at a random position and orientation inside the bounding box in the *cis* chamber and ends when the particle translocates into the *trans* chamber *via* the nanopore. This way, we are able to determine the capsule's dynamics in the nanopore ($0 < z < L$) including how frequently it rotates during the translocation process. About 1600 translocation simulations for each set were executed, ranging between approximately 800 to 6000 CPU hours of computational time for all simulations for each case (due to the total translocation time dependency on the simulation conditions). An example of a single simulation showing the capsule's center of mass trajectory while inside the nanopore is shown in Fig. 3. We can see that in this particular case the particle tends to move along the wall. This trace shows that the particle is most likely to be located near the membrane surface due to the electrostatic attraction between the negatively charged particle and nanopore with effectively positive charge.

Fig. 4 shows how a capsule's orientation in the pore (defined through the angle θ between the particle major axis and nanopore axis, see Fig. 2) is influenced by particle size and charge, pore size, and membrane bias. Regardless of the particle charge and/or membrane bias, the capsule is discouraged from rotating away from the pore axis when the particle's length increases, as demonstrated by the increase of the probability $P(\Omega)$ of the capsule's angle θ at $\theta \rightarrow 0^\circ(180^\circ)$ when comparing N = 5 (Fig. 4(a)) to N = 11 (Fig. 4(b and c)) because of the repulsion from the membrane surface preventing longer particles from exhibiting a horizontal orientation (in xy-plane). Also, for all cases considered in Fig. 4, the capsule's major axis is most often oriented along the pore axis when $q_i = -2e$ and V_m = 1 V (a similar but less prominent trend also emerges when $q_i = -1e$ and V_m = 1 V, not shown). This is due to the particle's attraction toward the membrane surface inside the pore, which in turn restricts its ability to rotate near the wall (and therefore its propensity to tumble, see Section 3.3).

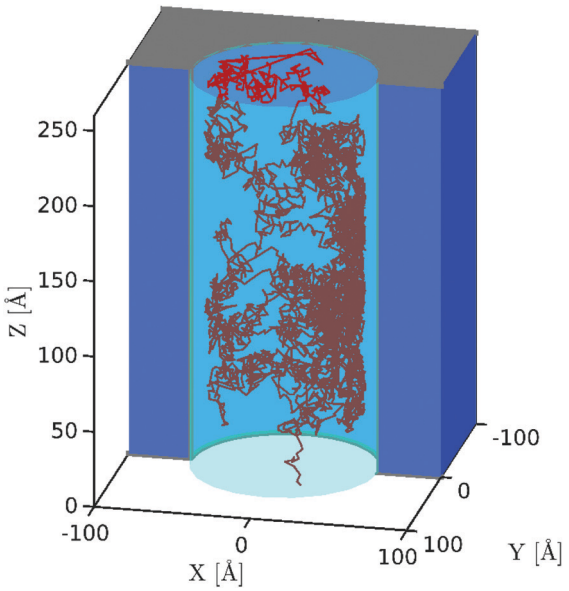

Fig. 3 Capsule center of mass motion over the course of a single simulation ($q_i = -2e$, V_m = 1 V, N = 5, R_p = 60 Å) while the particle is inside of the pore.

When the capsule length is small compared to the pore radius ($L_c < R_p$), the particle's probability $P(\Omega)$ is weakly dependent on θ for $V_m = -1$ V regardless of its charge, also seen in Fig. 4(a and c). This is because in this case the particles are discouraged from being close to the wall (due to the LJ and repulsive electrostatic interactions for $q_i \neq 0$) and there is enough space inside the pore for the capsule to rotate. This is not so for more narrow pores, as seen in Fig. 4(b) when R_p = 40 Å and N = 11 (L_c = 60 Å). When the capsules are more restricted in their rotational movement, the neutral particle with q_i = 0 is less likely to be oriented along the pore axis compared to the negatively charged particle subject to negative membrane bias because in this case the effective pore radius is smaller so that it becomes more difficult for the particle to rotate and the probability $P(\Omega)$ of finding the particle oriented along the pore axis ($\theta \rightarrow 0^\circ$ or 180°) increases.

To understand where capsule's are positioned in the nanopore, histograms for the probability of the capsule's radial center of mass location in the pore (R_{cm}) for annuli of equal area in the xy-plane, $P(A_{xy})$, are computed (Fig. 5). The radial position of the particle while in the pore for $q_i = -2e$, V_m = 1 V, N = 5, R_p = 40 Å, Fig. 5(a), reveals that the capsule's center of mass has the highest probability of being located toward the membrane surface. When $q_i = -2e$ for $V_m = -1$ V (Fig. 5(a)), the $P(A_{xy})$ is large near the center of pore, as the capsule is repelled from the membrane surface. This trend is less obvious for $q_i = -1e$ (Fig. 5(b)), where the particle's peak probability is still located close to the membrane wall but the maximum $P(A_{xy})$ is halved compared to the $q_i = -2e$ case, and the particle spends significantly more time near the

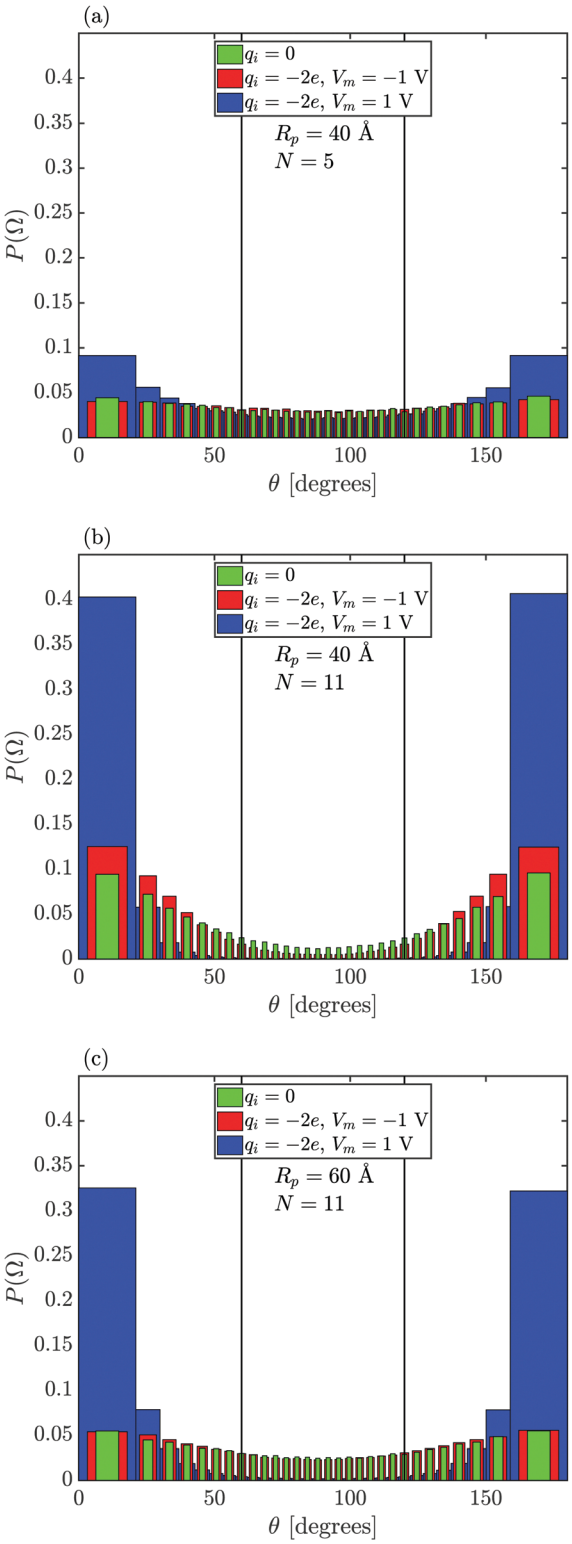

Fig. 4 The probability of the capsule's orientation angle θ while in the pore (computed using equal solid angles Ω), $P(\Omega)$, for $q_i = -2e$ at $V_m = \pm 1$ V, and $q_i = 0$, in the following cases: (a) $R_p = 40$ Å, $N = 5$ ($L_c = 30$ Å), (b) $R_p = 40$ Å, $N = 11$ ($L_c = 60$ Å), (c) $R_p = 60$ Å, $N = 11$ ($L_c = 60$ Å). The solid lines indicate angles $\theta_{up} = 60^\circ$ and $\theta_{down} = 120^\circ$ (see Section 3.3).

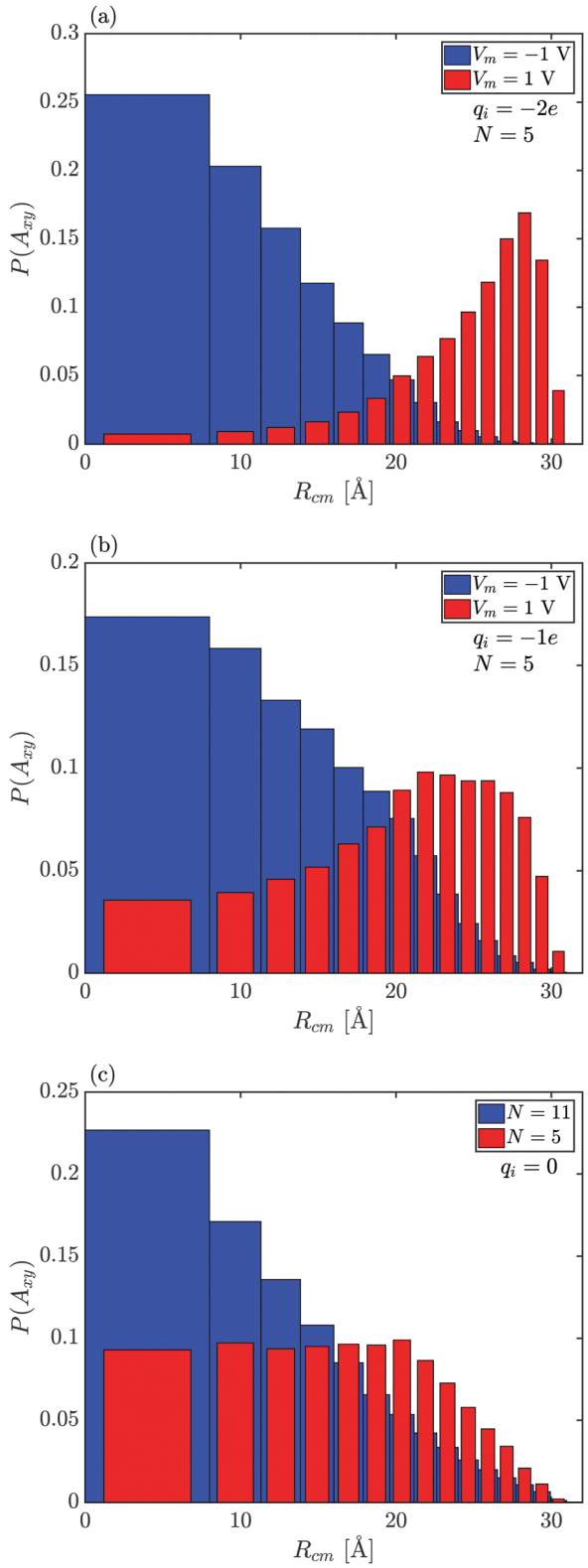

Fig. 5 The probability of the capsule's center of mass location $P(A_{xy})$ in the radial direction, R_{cm}, while inside the pore (using computed equal area A_{xy} concentric circles) for pore radius $R_p = 40$ Å. (a) $q_i = -2e$ ($N = 5$), $V_m = \pm 1$ V, (b) $q_i = -1e$ ($N = 5$), $V_m = \pm 1$ V, (c) $q_i = 0$, $N = 5$ and $N = 11$.

center of the pore. This is because the attractive electric interaction in this case is not strong enough to overcome the stochastic

effects and repulsive particle–membrane LJ interaction, and therefore, a particle will have a non-negligible probability of being found towards the center of the pore.

For a small neutral particle that can more freely rotate inside the nanopore ($N = 5$ in Fig. 5(c)), $P(A_{xy})$ remains nearly constant until the particle is close enough to the membrane wall, and $P(A_{xy}) \to 0$. In Fig. 5(c), it is also seen for a long neutral particle ($N = 11$) that $P(A_{xy})$ is larger for smaller R_{cm}, as a longer particle will have a tendency to orient itself along the pore axis (see Fig. 4(b)) with the capsule's center of mass near the pore center.

3.2 Translocation dynamics

Next, we consider how capsule's translocation time, t_t, depends on its length and charge. We define translocation time as the time it takes for a capsule to move from the *cis* chamber into the *trans* chamber *via* the nanopore in one successful attempt (without returning back to the *cis* chamber). The average translocation times $\langle t_t \rangle$ *vs.* pore radius R_p for select capsule sizes ($N = 5$, $N = 9$, and $N = 11$) are shown in Fig. 6. For all cases observed, smaller capsule sizes and increased pore radius result in a shorter $\langle t_t \rangle$. This is due to the shorter capsules having a smaller drag coefficient, reduced LJ particle–wall interactions, and a reduced electrostatic interaction with the wall compared to larger capsules in a more confined space of nanopores with smaller radius.

When the capsule and membrane are both negatively charged (or the capsule is neutral), translocation times are the lowest with similar values (~ 1 μs) which do not increase significantly with the bead's number N. This result is due to capsules being repelled from the pore walls, producing quick translocations but with many failed translocation attempts. The fact that $\langle t_t \rangle$ for negatively charged particles and $V_m < 0$ is very close to the values for the neutral particle suggests that the particles are driven by free diffusion along the pore's axis. In this case, $\langle t_t \rangle \approx L^2 \xi_\parallel / 6 k_b T$ (shown by a horizontal dashed line in Fig. 6) for most capsule sizes independent of the pore radius, and consistent with results for the mean first passage times[45].

On the other hand, when the applied membrane bias is positive, $V_m > 0$, the particle's motion is inhibited so that the translocation times are longer, and there are fewer failed attempts to translocate from the *cis* into the *trans* chamber since the particle is attracted to the pore surface, making it less likely for the capsule to escape from either end of the pore once inside. As can be observed from Fig. 6, in this case the average translocation time changes linearly with the particle's net particle charge, $\langle t_t \rangle \propto N q_i$ when $q_i = -1e$ and $\langle t_t \rangle \propto \exp(N q_i)$ for $q_i = -2e$ resulting in a dramatic increase in translocation time values (~ 40 μs for $q_i = -2e$ *vs.* ~ 2.5 μs for $q_i = -1e$, $N = 11$, for example). The escalation of the average translocation time values can be attributed to the capsule's electrostatic interaction with the membrane being the dominating factor in its motion through the pore (corresponding to the biased diffusion case[45]), especially for longer capsules and smaller pores since in this case the capsule is forced to be oriented along the pore axis more often which encourages strong capsule–pore interactions (the particles effectively "sticks" to the wall along the

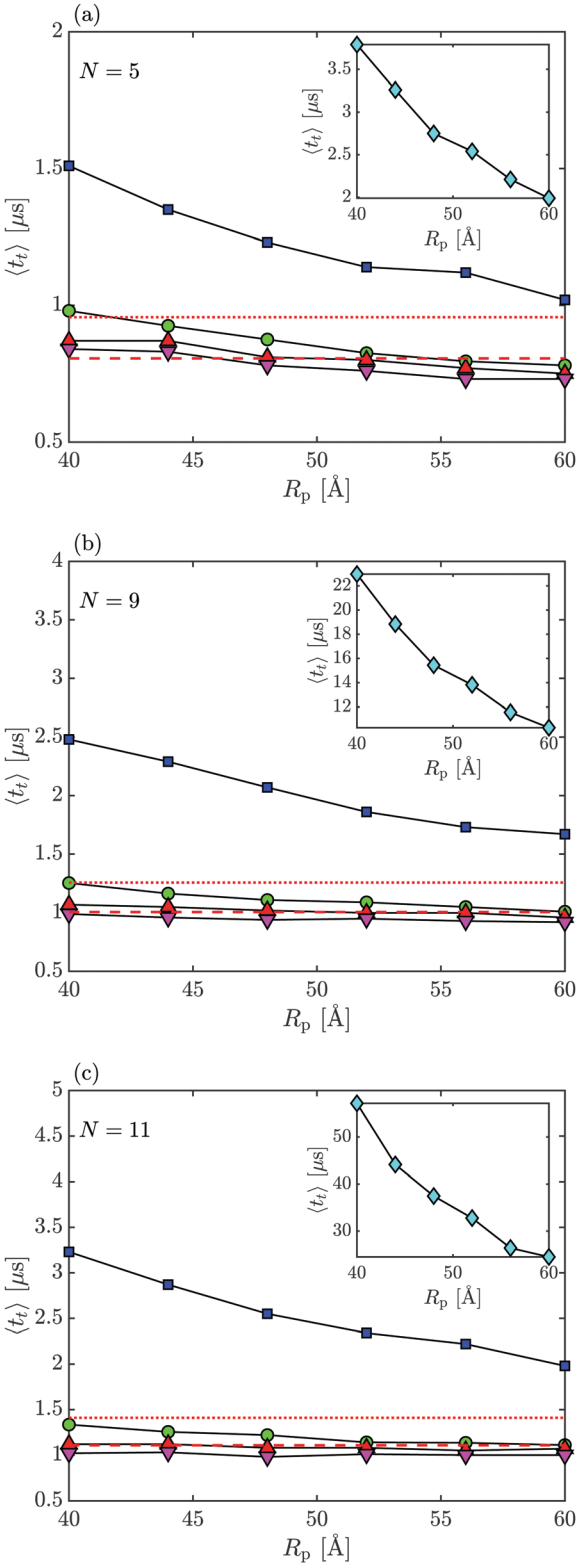

Fig. 6 The capsule's average translocation time, $\langle t_t \rangle$ *vs.* nanopore radius R_p for (a) $N = 5$, (b) $N = 9$, and (c) $N = 11$: (▽) $V_m = -1$ V, $q_i = -2e$; (Δ) $V_m = -1$ V, $q_i = -1e$; (○) $q_i = 0$; (□)) $V_m = 1$ V, $q_i = -1e$; (◊) $V_m = 1$ V, $q_i = -2e$ (inset). The horizontal dashed and dotted line correspond to free diffusion times $L^2 \xi_\parallel / 6 k_b T$ and $L^2 \xi_\perp / 6 k_b T$, respectively.

entire length of the particle). Note also a strong dependence of the translocation time on the pore radius: As R_p decreases, the translocation time increases which is consistent with the particle–pore interaction becoming stronger with decreasing curvature of the pore.

3.3 Tumbling dynamics

Next, we focus on how the membrane bias, the pore radius, and size/charge of the capsule affect the particle's tumbling dynamics as it translocates through the nanopore. Using the orientation angle θ between the capsule's major axis and the pore's axis (see Fig. 2 and Section 3.1), a single "tumble" is defined by the capsule's major axis rotating from an upper threshold ($\theta_{up} = 60^\circ$) to a lower threshold ($\theta_{down} = 120^\circ$) orientation or *vice versa*. These values of $\theta_{up(down)}$ were chosen since for a freely moving particle (subjected only to a stochastic force), the expectation value, $\langle\theta\rangle$, for $0^\circ < \theta < 90^\circ$ is $\langle\theta\rangle = \int_0^{\pi/2}\theta\sin(\theta)\mathrm{d}\theta = 1$ rad $\approx 60^\circ$ ($\langle\theta\rangle = \int_{\pi/2}^{\pi}\theta\sin(\theta)\mathrm{d}\theta = (\pi - 1)$ rads $\approx 120^\circ$ when $90^\circ < \theta < 180^\circ$).

The average time required for the capsule to rotate from θ_{up} to θ_{down} successfully in a single attempt, $\langle t_s\rangle$, is primarily determined by the free rotational diffusion when $\langle t_s\rangle \approx \xi_R(\theta_{up} - \theta_{down})^2/6k_bT$. Since longer capsules have a larger value of ξ_R, $\langle t_s\rangle$ increases from 0.8 ns for $N = 3$ to 7.0 ns for $N = 11$ (see inset in Fig. 7 for $N = 5$, histograms for other N are similar). Despite capsules with the same N but different charges and in different electrostatic environments having similar $\langle t_s\rangle$ values, the frequency of tumbling inside the nanopore exhibited by these particles can differ greatly. Therefore, an average time for a particle to tumble that includes the particle's failed tumbling attempts, referred to as $\langle t_\theta\rangle$, is much greater than t_s, as seen in Fig. 7, and is considerably more dependent on the system's parameters.

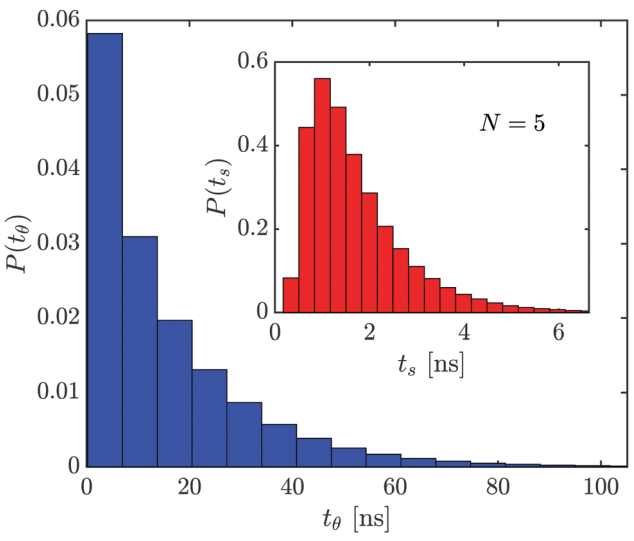

Fig. 7 Histograms of total tumbling times, t_θ, and (inset) only successful tumbling attempts, t_s, for $N = 5$, $q_i = -2e$ capsules in a $R_p = 40$ Å, $V_m = 1$ V pore. The averages $\langle t_\theta\rangle$ and $\langle t_s\rangle$ extracted from the histograms are 15.5 and 1.7 ns, respectively.

To establish how the capsule's tumbling dynamics is influenced by nanopore system properties, we investigate the

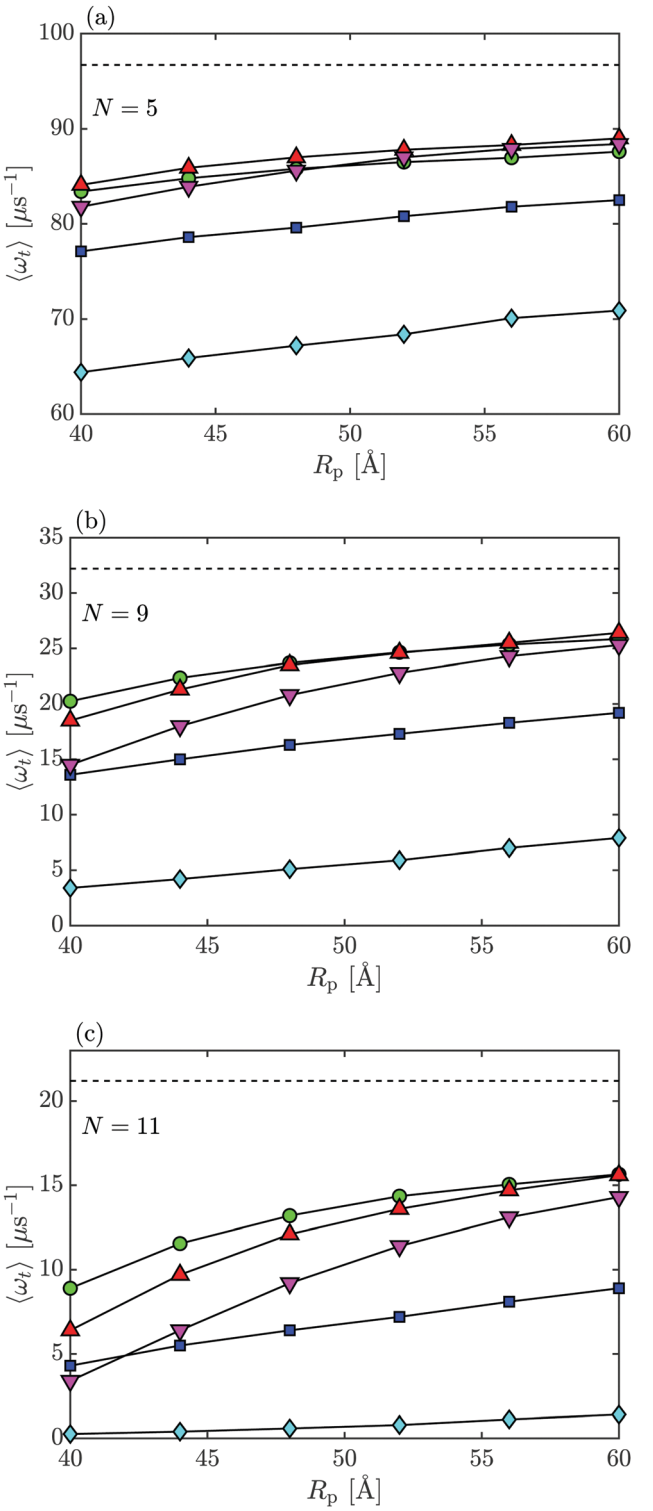

Fig. 8 The capsule's tumbling rate, $\langle\omega_t\rangle$, for $R_p = 40$ Å to 60 Å for parameters: (▽) $V_m = -1$ V, $q_i = -2e$; (Δ) $V_m = -1$ V, $q_i = -1e$; (○) $q_i = 0$; (□)) $V_m = 1$ V, $q_i = -1e$; (◊) $V_m = 1$ V, $q_i = -2e$; dashed line is for $q_i = 0$ in free space (outside of the pore). The capsule lengths studied include (a) $N = 5$, (b) $N = 9$, and (c) $N = 11$.

average tumbling rate, *i.e.*, the number of tumbles per μs, $\langle\omega_t\rangle = 1/\langle t_\theta\rangle$, for each set of parameters. For all cases studied, the $\langle\omega_t\rangle$ of the capsule in the bulk is higher compared to $\langle\omega_t\rangle$ inside of the nanopore (see Fig. 8 where the dashed line is for the bulk). We can also see in Fig. 8 that the shorter the capsule (smaller N), the higher the $\langle\omega_t\rangle$, due to the smaller rotational drag and less number of attempts needed to complete a tumble. Additionally, a more narrow pore exhibit smaller $\langle\omega_t\rangle$, revealing how a more confined space reduces the ability for the capsule to tumble.

For most cases studied, particularly those with larger N, the tumbling rate $\langle\omega_t\rangle$ for the neutral particle was higher than for capsules with $q_i = -1e$, $V_m = 1$ V, which in turn had higher $\langle\omega_t\rangle$'s than for $q_i = -2e$, $V_m = 1$ V cases. The cases with $q_i = -2e$ exhibit a particular sharp drop in tumbling rates from $\sim 65\ \mu s^{-1}$ for $N = 5$ to $\sim 0.25\ \mu s^{-1}$ for $N = 11$. As discussed earlier, the capsule's "sticking" to the membrane wall discourages rotations (see Fig. 4 and 5), which is why long capsules with charge $q_i = -2e$ tumble the least.

On the other hand, the effects that N, R_p, and q_i have on the $\langle\omega_t\rangle$ for a negatively biased membrane are not as straightforward. For small N ($N = 5$, Fig. 8(a)), the rate of tumbling for negatively charged particles in a $V_m = -1$ V pore is about the same (it is even slightly higher for $N = 3$, not shown) as $\langle\omega_t\rangle$ for a neutral capsule. A trend begins to emerge when the capsule becomes longer ($N = 9$, Fig. 8(b)) and pore radius decreases ($R_p = 40$ Å) in which case, $q_i = -2e$ particles have a smaller $\langle\omega_t\rangle$ than capsules with $q_i = -1e$ as well as the neutral particle case. As N increases further, this difference in tumbling rates extends to larger pore radii, see Fig. 8(c) for $N = 11$.

When $V_m = -1$ V, the particle is repelled from the membrane surface *via* the electrostatic repulsion as well as the particle–membrane LJ interactions. For smaller capsules, the repulsion has little effect on the tumbling rate because it can easily rotate completely regardless of its position in the nanopore. When N increases, the particle's ability to freely rotate becomes inhibited as the effective pore radius for the negatively charged particles subject to a negative membrane bias is much smaller than for the neutral particle. As a result, it becomes more difficult for the capsule to have angle θ to change by a large amount from $\langle\theta_{up}\rangle$ to $\langle\theta_{down}\rangle$ to ensure a full rotation and hence, the tumbling rate decreases.

By combining the data presented in Fig. 6 and 7, we also note that despite the fact the lowest tumbling rates occur for the opposite effective charges on the particle and the membrane (when $q_i < 0$, and $V_m = 1$ V), the total average number of rotations during a translocation time is larger in this case than when $V_m = -1$ V (~ 10 *vs.* 4 for $N = 11$, $q_i = -2e$, $V_m = 1$ V and $V_m = -1$ V). This is due to an increase in time it takes the capsule to go through the pore with the particle spending most of the time being "stuck" next to the membrane surface and only occasionally managing to rotate.

4 Concluding remarks

In this work, we studied the interactions that affect cylindrical capsule-like particles orientation and motion through a solid-state nanopore. The movement of rigid, rod-like structures comprised of overlapping spherical beads is modeled using a BD method alongside a PNP approach. We investigated how the applied membrane bias, pore radius, and particle size/charge relate to capsule location and orientation while translocating the nanopore. The purpose of considering these parameters and the resulting particle dynamics were to reveal how they contribute to the particle's propensity to tumble inside the nanopore.

We find that the parameter that influences the tumbling frequency the most is the particle's size, with shorter capsules rotating more frequently than longer capsules. However, other factors such as pore width also play a role, resulting in smaller tumbling rates due to the space confinement. We also find that neutral capsules tend to not favor any particular orientations if they are short but will mostly align itself along the pore axis if they are long compared to the nanopore radius.

The particle–membrane LJ interactions influence charged capsules in a similar way to neutral capsules, but the electric force changes the particle dynamics in those cases. For negative particles subjected to a positive membrane bias, the attraction toward the wall results in the capsule typically orienting itself along the pore axis. These trends are emphasized for longer and more negatively charged particles resulting in the decrease of the particle's rate of tumbling while greatly increasing the time it takes for it to translocate the nanopore.

The dynamics of negatively charged particles subjected to a negative membrane bias is not as intuitive. For short capsules/wide pores, such particles have the largest tumbling frequencies, close to bulk values ($\sim 10\%$ lower). When the capsule is longer (or the pore is more narrow), the rate of tumbling decreases. Furthermore, the capsules with a greater negative charge tumble less as the electrostatic interaction focuses particle motion along the pore's axis precluding its frequent rotations. This focusing also affects the translocation time, resulting in it being governed by free diffusion independent of the capsule's length and charge.

Conflicts of interest

There are no conflicts to declare.

Acknowledgements

This work was supported by the NSF through a CAREER award No. 1352218 (M. G.). We would like to acknowledge the use of Orion cluster at Clarkson University.

References

1 M. Firnkes, D. Pedone, J. Knezevic, M. Doblinger and U. Rant, *Nano Lett.*, 2010, **10**, 2162.
2 L.-Q. Gu and J. W. Shim, *Analyst*, 2010, **135**, 441.
3 A. de la Escosura-Muñiz and A. Merkoçi, *ACS Nano*, 2012, **6**, 7556.

4 D. H. Stoloff and M. Wanunu, *Curr. Opin. Biotechnol.*, 2013, **24**, 699.
5 Y. Feng, Y. Zhang, C. Ying, D. Wang and C. Du, *Genom., Proteom. Bioinform.*, 2015, **13**, 4.
6 D. Fologea, B. Ledden, D. S. McNabb and J. Li, *Appl. Phys. Lett.*, 2007, **91**, 053901.
7 L. Movileanu, *Trends Biotechnol.*, 2009, **27**, 333.
8 P.-H. Lee, V. Helms and T. Geyer, *J. Chem. Phys.*, 2012, **137**, 145105.
9 M. Muthukumar, *J. Chem. Phys.*, 2014, **141**, 081104.
10 J. Larkin, R. Y. Henley, M. Muthukumar, J. K. Rosenstein and M. Wanunu, *Biophys. J.*, 2014, **106**, 696.
11 H. Arjmandi-Tash, L. A. Belyaeva and G. F. Schneider, *Chem. Soc. Rev.*, 2016, **45**, 476.
12 J. J. Kasianowicz, E. Brandin, D. Branton and D. W. Deamer, *Proc. Natl. Acad. Sci. U. S. A.*, 1996, **93**, 13770.
13 R. M. Smeets, U. F. Keyser, D. Krapf, M.-Y. Wu, N. H. Dekker and C. Dekker, *Nano Lett*, 2006, **6**, 89.
14 M. Wanunu, J. Sutin, B. McNally, A. Chow and A. Meller, *Biophys. J.*, 2008, **95**, 4716.
15 Y. Qiu, P. Hinkle, C. Yang, H. E. Bakker, M. Schiel, H. Wang, D. Melnikov, M. Gracheva, M. E. Toimil-Molares and A. Imhof, *et al.*, *ACS Nano*, 2015, **9**, 4390.
16 Y. Zhang, M. A. Edwards, S. R. German and H. S. White, *J. Phys. Chem. C*, 2016, **120**, 20781.
17 S. Howorka and Z. Siwy, *Chem. Soc. Rev.*, 2009, **38**, 2360.
18 D. S. Talaga and J. Li, *J. Am. Chem. Soc.*, 2009, **131**, 9287.
19 C. Plesa, S. W. Kowalczyk, R. Zinsmeester, A. Y. Grosberg, Y. Rabin and C. Dekker, *Nano Lett*, 2013, **13**, 658.
20 Z. Hu, M. D. Fischbein, C. Querner and M. Drndić, *Nano Lett*, 2006, **6**, 2585.
21 M. Ali, R. Neumann and W. Ensinger, *ACS Nano*, 2010, **4**, 7267.
22 Y. Ai and S. Qian, *Phys. Chem. Chem. Phys.*, 2011, **13**, 4060.
23 H. Wu, Y. Chen, Q. Zhou, R. Wang, B. Xia, D. Ma, K. Luo and Q. Liu, *Anal. Chem.*, 2016, **88**, 2502.
24 A. J. McMullen, J. X. Tang and D. Stein, *ACS Nano*, 2017, **11**, 11669.
25 J. Sha, W. Si, B. Xu, S. Zhang, K. Li, K. Lin, H. Shi and Y. Chen, *Anal. Chem.*, 2018, **90**, 13826.
26 R. Maugi, P. Hauer, J. Bowen, E. Ashman, E. Hunsicker and M. Platt, *Nanoscale*, 2020, **12**, 262.
27 K. E. Venta, M. B. Zanjani, X. Ye, G. Danda, C. B. Murray, J. R. Lukes and M. Drndic, *Nano Lett*, 2014, **14**, 5358.
28 S. K. Kannam, S. C. Kim, P. R. Rogers, N. Gunn, J. Wagner, S. Harrer and M. T. Downton, *Nanotechnology*, 2014, **25**, 155502.
29 W. Si and A. Aksimentiev, *ACS Nano*, 2017, **11**, 7091.
30 A. Ammenti, F. Cecconi, U. Marini Bettolo Marconi and A. Vulpiani, *J. Phys. Chem. B*, 2009, **113**, 10348.
31 F. Cecconi, M. Bacci and M. Chinappi, *Protein Pept. Lett.*, 2014, **21**, 227.
32 I. Jou and M. Muthukumar, *Biophys. J.*, 2017, **113**, 1664.
33 Z. Liu, X. Shi and H. Wu, *Nanotechnology*, 2019, **30**, 165701.
34 X. Sun, T. Lin and J. D. Gezelter, *J. Chem. Phys.*, 2008, **128**, 234107.
35 A. Nadtochiy, D. Melnikov and M. Gracheva, *ACS Nano*, 2013, **7**, 7053.
36 I. A. Jou, D. V. Melnikov and M. E. Gracheva, *Nanotechnology*, 2016, **27**, 205201.
37 M. E. Gracheva, J. Vidal and J.-P. Leburton, *Nano Lett*, 2007, **7**, 1717.
38 C. C. Wells, D. V. Melnikov and M. E. Gracheva, *J. Chem. Phys.*, 2019, **150**, 115103.
39 A. Nikolaev and M. E. Gracheva, *Nanotechnology*, 2011, **22**, 165202.
40 M. M. Tirado, C. L. Martnez and J. G. de la Torre, *J. Chem. Phys.*, 1984, **81**, 2047.
41 H. Löwen, *Physical Review E*, 1994, **50**, 1232.
42 C. C. Wells, D. V. Melnikov, J. T. Cirillo and M. E. Gracheva, *Physical Review E*, 2020, **102**, 063104.
43 D. L. Ermak and J. McCammon, *J. Chem. Phys.*, 1978, **69**, 1352.
44 N. Watari, M. Doi and R. G. Larson, *Physical Review E*, 2008, **78**, 011801.
45 S. Redner, *A guide to first-passage processes*, Cambridge University Press, 2001.